Sound source localization technique using a seismic streamer and its extension for whale localization during seismic surveys

Shima H. Abadi[a)]
Lamont–Doherty Earth Observatory, Columbia University, Palisades, New York 10964, USA

William S. D. Wilcock
School of Oceanography, University of Washington, Seattle, Washington 98195, USA

Maya Tolstoy, Timothy J. Crone, and Suzanne M. Carbotte
Lamont–Doherty Earth Observatory, Columbia University, Palisades, New York 10964, USA

(Received 17 July 2014; revised 17 November 2015; accepted 30 November 2015; published online 30 December 2015)

Marine seismic surveys are under increasing scrutiny because of concern that they may disturb or otherwise harm marine mammals and impede their communications. Most of the energy from seismic surveys is low frequency, so concerns are particularly focused on baleen whales. Extensive mitigation efforts accompany seismic surveys, including visual and acoustic monitoring, but the possibility remains that not all animals in an area can be observed and located. One potential way to improve mitigation efforts is to utilize the seismic hydrophone streamer to detect and locate calling baleen whales. This study describes a method to localize low frequency sound sources with data recoded by a streamer. Beamforming is used to estimate the angle of arriving energy relative to sub-arrays of the streamer which constrains the horizontal propagation velocity to each sub-array for a given trial location. A grid search method is then used to minimize the time residual for relative arrival times along the streamer estimated by cross correlation. Results from both simulation and experiment are shown and data from the marine mammal observers and the passive acoustic monitoring conducted simultaneously with the seismic survey are used to verify the analysis.
 [http://dx.doi.org/10.1121/1.4937768]

[AMT] Pages: 3951–3963

I. INTRODUCTION

Animal localization is important for studying the impact of different anthropogenic sounds on marine mammals. Active sonar, transportation, geophysical surveys, and construction are among the most common man made sounds that may impact marine mammals (McKenna *et al.*, 2012; Bassett *et al.*, 2012; Richardson *et al.*, 1995). The high sound source levels involved in seismic reflection surveys have raised concern over their effects on marine life (e.g., Gordon *et al.*, 2004). Seismic reflection surveys use low frequency acoustic energy to image the structure of the seafloor, with seismic arrays designed to focus as much of the sound as possible downward to maximize the energy penetrating the solid earth (Diebold *et al.*, 2010). To better mitigate against any potential impacts of seismic sources, broadband measurements of acoustic received levels have been made to quantify the exposure level (Tolstoy *et al.*, 2004; Tolstoy *et al.*, 2009; Diebold *et al.*, 2010). Thus safety radii and exposure radii can be established for a given seismic source array design, based on the criteria defined by the National Marine Fisheries Service. Recent work has shown it may be possible to establish safety radii in near-real time utilizing the seismic streamer (Crone *et al.*, 2014), thus better accounting for site specific geological variability. During each seismic experiment, experienced marine mammal observers monitor the safety radii visually and acoustically with a short hydrophone array and seismic operations are suspended if mammals enter the safety zone. However, further acoustic monitoring, and in particular, the ability to locate marine mammal calls, could be used to demonstrate the effectiveness of the observations and might add an additional level of safety to existing methods.

Several sound source localization techniques have been developed to locate and track marine mammals underwater. Many passive acoustic monitoring techniques use multipath arrival times for locating marine mammals (e.g., McDonald *et al.*, 1995; Wilcock, 2012). The time differences of arrivals from large numbers of widely distributed time-synchronized receivers can also be used for estimating the marine mammal's location (e.g., Speisberger and Fristrup, 1990; Clark and Ellison, 2000; Nosal and Frazer, 2006). Some techniques can locate multiple sources using the time differences of arrivals without source separation (e.g., Nosal, 2013). Triangulation is another technique, which uses the azimuth of sounds from several distributed recorders to locate marine mammals in shallow water (e.g., Greene *et al.*, 2004; Thode *et al.*, 2012). The U.S. Navy's SOund SUrveillance System was also used to detect and locate blue whale calls in the northeast Pacific using the arrival times derived from the matched filter output (Stafford *et al.*, 1998).

There are several localization techniques which use signals recorded by a single sensor. Normal mode modeling is a

[a)]Also at: School of Oceanography, University of Washington, Seattle, WA 98195. Electronic mail: abadi@columbia.edu

useful technique to estimate the range of marine mammals when only one recording instrument is available (Wiggins *et al.*, 2004). Multipath arrival information can also be used for whale localization using a single recorder (Tiemann *et al.*, 2006; McDonald and Fox, 1999).

Several sound source localization techniques use a vertical hydrophone array for locating sound sources. Sequential Bayesian filtering has been applied to underwater target tracking (Yardim *et al.*, 2011). Adaptive modal backpropagation is a localization technique that matches the amplitude and phase of the isolated modes with the modeled propagation modes (Lin *et al.*, 2012). Matched-Field Processing (MFP) is another sound source localization technique that matches the measured field at the array with replicas derived by a propagation model for all source locations (Jensen *et al.*, 1994; Bucker, 1976). MFP has also been used to successfully localize marine mammals (Thode *et al.*, 2000; Thode *et al.*, 2006). A single linear vertical array has been used to locate marine mammals in shallow water by isolating the different modal arrivals (Abadi *et al.*, 2014).

A linear horizontal array can also be used for sound source localization. The waveguide invariant is used to estimate the range of an underwater sound source using a towed acoustic receiver (Cockrell and Schmidt, 2010). The waveguide invariant method uses the constant slope of the underwater acoustic intensity striations mapped in range and frequency. Array invariant is another method to estimate the source range using the data recorded by a horizontal array in shallow water (Lee and Makris, 2006). The array invariant method has been compared to the moving array triangulation (MAT) and the bearings-only target motion analysis using a towed horizontal receiver (Gong *et al.*, 2013).

There is a significant body of literature on using towed acoustic arrays in marine mammal localizations. The MAT technique has been used for estimating the range of sperm whales (Tran *et al.*, 2014). The effect of towed array stability on marine mammal localization using the triangulation technique has been studied by applying a linear perturbation analysis to the ranging equations (von Benda-Beckmann *et al.*, 2013). The effect of sonar on humpback calls has been investigated by finding the whale bearings using beamforming and their ranges using instantaneous array invariant method and synthetic aperture tracking techniques (Gong *et al.*, 2014). A short horizontal array towed at 100 m depth has been used to estimate sperm whale abundance from a combined acoustic and visual survey (Barlow and Taylor, 2005). Two miniature acoustic data-loggers have been used to detect, localize, and track the high-frequency echolocation click events of finless porpoises (Li *et al.*, 2009). The relative arrival times between the direct and surface reflected paths, measured by two- or three-element vertical or horizontal arrays, can be used to track sperm whales (Thode, 2004) and this method has been extended to account for the refraction of rays arising from a depth-dependent sound speed (Thode, 2005).

The purpose of this paper is to develop and evaluate a technique to locate a low-frequency short-duration underwater sound source using a long horizontal array of sensors (in this case an 8-km long multi-channel seismic streamer) and expand it to whale localization in the vicinity of seismic surveys. The remainder of this paper is divided into five sections. Section II describes the seismic experiment, associated visual and acoustic monitoring surveys, and the signals received by the streamer. Section III presents the mathematical formulation of the sound source localization technique. Section IV presents the sound source localization results from simulated normal mode propagation in a simple environment that mimics the seismic experiment. Section V presents the localization results for the airgun signals and the whale calls. Section VI summarizes the conclusions of the study.

II. 2012 COAST EXPERIMENT

The data utilized in this paper are from the COAST (Cascadia Open-Access Seismic Transects) seismic reflection experiment (Holbrook *et al.*, 2012) conducted by the *R/V Marcus G. Langseth* on cruise MGL1212, from July 12–24, 2012. This experiment spanned a wide range of water depths from the continental shelf (~40 m) to deep water (~2600 m). Figure 1(a) shows a map of this experiment. The survey includes 12 main track lines including 9 east–west lines across the continental slope, 2 north–south lines along the strike of the continental margin and one line (A/T) northeast of the main survey area on the continental shelf. The shooting started with line 11, turned south to do the odd lines (1, 3, 5, 7, 9), turned north to do the even lines (8, 6, 4, 2) and the A/T line, and then finished with line 10. During turns

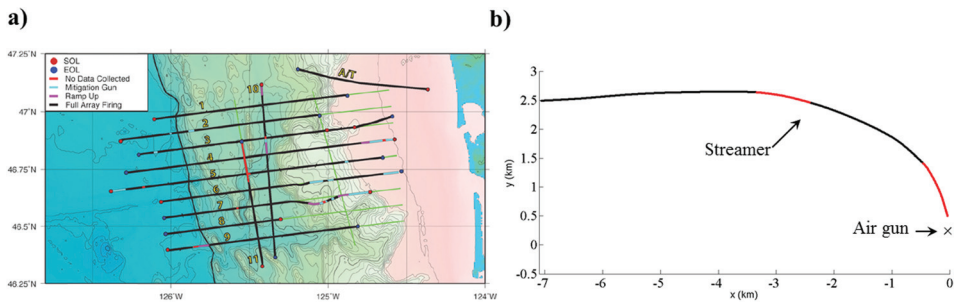

FIG. 1. (a) Map of the COAST cruise track lines showing the gun array status during shooting. Thick black lines show where the full array was shooting, light blue lines show where only the mitigation gun was shooting, and the purple lines show the location of ramp up periods from shut down or mitigation gun to the full array shooting. Red and blue circles show the start of lines and end of lines, respectively. (b) The location of all receivers relative to the vessel (for the seventh shot in Table IV). The cross shows the location of the airgun array. The sections of the streamer that cannot be used for localization because of the end-fire effect or streamer curvatures are shown in red.

between track lines where data are not useful for imaging or when a marine mammal was observed in the area, the seismic source was powered down to the mitigation gun (40 cubic inches airgun) to avoid unnecessary disturbance to the marine environment [light blue sections in Fig. 1(a)]. All the experimental data used in this study comes from turns between track lines when the mitigation gun was being used.

The purpose of the cruise was to acquire a grid of two-dimensional seismic reflection profiles and associated geophysical data in a corridor off Grays Harbor, Washington along the Cascadia Subduction Zone, as part of the U.S. National Science Foundation's GeoPRISMS program. Details of the source and receiver arrays, the acoustic and visual monitoring surveys conducted on the *R/V Langseth* and accompanying vessel *Northern Light*, and the signals recorded by the streamer are provided below.

A. Source and receiver arrays

The seismic source array used on this cruise had 36 airguns with a total volume of 6600 cubic inches. The airgun shots occurred every 50 m while the ship moved at a speed of ~4.5 knots, equivalent to a shooting interval of ~22 s. After each shot hydrophone data from the streamer were recorded for 16 s. Since the ship moves only ~37 m over the 16 s recording interval, the streamer is considered stationary during each shot record for the purposes of this research.

The seismic streamer is 8 km long and comprises 636 hydrophone channels that are spaced 12.5 m apart. For this study the streamer was towed at a constant depth of 9 m and recorded from each channel with a sampling rate of 500 Hz. Positions were determined for the source and each hydrophone channel for each shot using differential global positioning system observation on the vessel, seismic source array, and tail buoy, together with compass headings on the streamer and range and bearing data from transducers on the source, streamer, and tail buoy. The vessel position is known with sub-meter accuracy and the position error on the streamer varies from 1.5 to 4 m going from near to far hydrophone channels. The distance between the source and the near hydrophone and the far hydrophone is 265 and 7.38 km, respectively. Figure 1(b) shows the location of the source and the receiver arrays of the seventh shot considered in Sec. V.

B. Marine mammal monitoring surveys

All *R/V Langseth* cruises utilizing airguns conduct marine mammal monitoring surveys concurrent with the seismic experiment. The monitoring survey uses a combination of visual and acoustic watches to minimize potential impacts on marine mammals.

1. Visual monitoring survey

There were five trained and experienced Protected Species Observers (PSOs) on board the *R/V Langseth* to conduct the monitoring, record and report observations, and request mitigation actions. Visual monitoring was primarily carried out from an observation tower located 18.9 m above the sea surface, which afforded the PSOs a 360° view. When a protected species was observed, range estimates were made using reticle binoculars, the naked eye, and by relating the animal to an object at a known distance, such as the acoustic array located 232 m from the PSO tower. If the animal was inside the safety radius, the seismic technician would be notified to power down (to the 40 cubic inches mitigation gun) or shut down the source (all guns are off). These two cases are associated with different start up procedures.

The visual monitoring effort on the *Langseth* yielded 92 protected species detection records; 84 for cetaceans and 8 for pinnipeds. The majority of mitigation downtime was attributable to humpback whales, with a total of 34 sightings during the survey. Four of these observations resulted in shut-downs, one sighting resulted in a power-down, and three sightings led to delayed ramp-ups to resume seismic operations.

During the start of the seismic survey and while the *Langseth* was in the area of the continental shelf, a contracted support vessel *Northern Light* monitored the area approximately 5 km to the north of the *Langseth*. The *Northern Light* has a flying bridge at height of 4.9–5.5 m above the sea surface that enabled observers to see around the entire vessel. It is possible to observe animals at a distance of approximately 5 to 6 km with the naked eye in optimal conditions. The *Northern Light* notified the *Langseth* when there was a protected species of interest inside or nearing the safety radius. The visual monitoring effort on the *Northern Light* yielded 174 protected species detection records.

2. Acoustic monitoring survey

Passive acoustics monitoring (PAM) was used to compliment the visual monitoring effort. The PAM system consists of a hydrophone array with four elements. Three of the hydrophone elements are broadband (2 to 200 kHz) and the fourth element is for sampling lower frequencies (75 Hz to 30 kHz). However, at frequencies less than 1 kHz, the PAM system was not effective for marine mammal detections due to the presence of ship noise.

C. Received signals

After the application of the anti-alias filter, the streamer records signals with frequencies up to ~220 Hz. The streamer is designed to record the airgun signal and its bottom reflected paths. Figure 2(a) shows an example spectrogram of a mitigation gun; the airgun signature is dominated by energy between 20 and 80 Hz (see Tolstoy *et al.*, 2009; Diebold *et al.*, 2010) and thus provides a useful signal to evaluate a method for locating a low frequency impulsive source.

In addition to the airgun signal, several low frequency sounds that are likely marine mammals were also recorded by the seismic streamer. Figures 2(b) and 2(c) show two examples of marine mammal signals recorded on July 16, 2012 that coincided with a period when humpback whales were observed in the vicinity of the experiment.

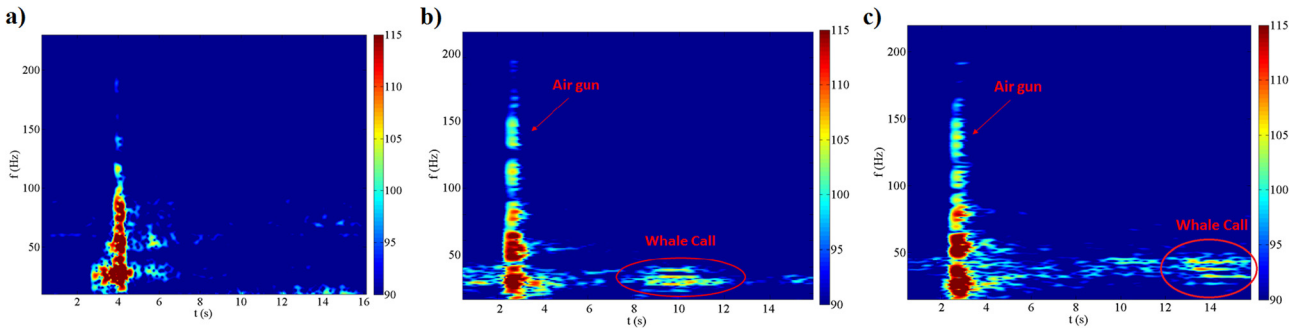

FIG. 2. (Color online) (a) Spectrogram of the mitigation gun recorded on July 16, 2012 at 17:59:47 (the seventh shot in Table IV), for an element 6.14 km from the center of the vessel, (b) the spectrogram of an airgun followed by a whale call recorded at 21:06:11 (the second call in Table VI), (c) the spectrogram of an airgun followed by a whale call recorded at 21:09:03 (the third call in Table VI).

The goal of this research is to use the streamer data to localize marine mammals (specifically baleen whales) during the seismic surveys. For this purpose, a low-frequency sound source localization method is developed and evaluated using simulations and the experiment data.

III. SOUND SOURCE LOCALIZATION TECHNIQUE USING SEISMIC STREAMER

To locate the low frequency sound sources three established methods were initially considered. The first, the array invariant method (Lee and Makris, 2006) can estimate range using passive beam-time intensity data in a horizontally stratified shallow water ocean waveguide (when the waveguide invariant β is equal to 1 from Song and Cho, 2015) provided the frequencies are not near the modal cutoff frequency of the most excited modes. This requirement is not satisfied for the application presented in this paper because either the recorded frequencies are near the modal cutoff frequencies of almost all modes in shallow water (see Sec. IV) or the waveguide invariant is not unity in deep water. Also, the array invariant technique requires a sufficiently large bandwidth while the sound sources presented in this study are narrow bandwidth signals.

The second method considered here is the triangulation of the beamformer outputs from each sub-array. This approach fails because not all modes propagate horizontally and the beamformer output is an averaged arrival angle of all the excited modes. This can be seen on the localization figures (see Sec. V) where the estimated source location differs from the beamforming intersection point.

The third method was a grid search technique based on the idea of near-field (curved wave-front) beamforming when the time delay associated with each element was calculated from an acoustic model. However, because the calculated time delay should be used in the phase of the conventional beamforming components and any small error (due to the noise or environmental mismatch) in phase may cause a large location uncertainty, this method is ineffective.

The technique developed in this paper assumes that the propagation of acoustic signals in the ocean can be approximated by traveling ray paths between the sound source and the receiver. It has been shown that ray theory fails in many ocean propagation situations particularly for low frequencies in shallow water (Kinsler *et al.*, 2000). However, studies show that ray theory can be used for shallow water at small ranges when it does not predict shadow zones (Pedersen and Gordon, 1965) and when the wavelength is small compared to the water depth (Jensen *et al.*, 1994). In this paper, it is shown that use of the ray theory for ranging low frequency sound sources recorded by a seismic streamer produces acceptable location errors for signals with large signal-to-noise ratios (SNRs).

In ray theory, the speed of sound decreases with depth in the ocean thermocline. So, there may be no direct path between a shallow source and a receiver at large ranges. In mode theory, each mode propagates with different group velocity at different elevation angles. Hence, the travel time cannot be directly calculated by dividing the range by the average speed of sound. Either the actual travel distance or the horizontal propagation speed needs to be known to calculate the propagation time. In this section we present a sound source localization method that first uses beamforming to infer that required horizontal propagation speed to each sub-array of the streamer for a given source location and then uses a grid search method to find the source location that minimizes the root-mean-square (rms) travel time residual for all sub-arrays. Note that this method does not provide any information about the source depth.

Considering the configuration illustrated in Fig. 3(a), a potential horizontal sound source location is denoted by (x_s, y_s) and each element of the receiver array by $(x_i, y_i)_j$, where j is the sub-array index $(1 \le j \le M)$, M is the total number of sub-arrays, i is the element index inside each sub-array $(1 \le i \le N_j)$, and N_j is the number of elements in the jth sub-array. Any ray traveling along a path between (x_s, y_s) and $(x_i, y_i)_j$, travels with the speed of sound. However, if the ray path is not horizontal, the intersection of the wave front and the sea surface travels at a slower velocity [Fig. 3(b)]. Thus, the calculated travel time between (x_s, y_s) and $(x_i, y_i)_j$, $t^c_{i,j}$, is different from the simple expression $(r_{i,j}/\bar{c})$, where $r_{i,j}$ is the distance between (x_s, y_s) and $(x_i, y_i)_j$, and $\bar{c}$ is the depth-averaged speed of sound from XCTD measurement during the cruise, and must instead be calculated from

$$t^c_{i,j} = \frac{r_{i,j}}{V_H} = \frac{\sqrt{(x_s - x_{i,j})^2 + (y_s - y_{i,j})^2}}{\bar{c}\,\sin[\varphi_j(x_s, y_s)]}, \tag{1}$$

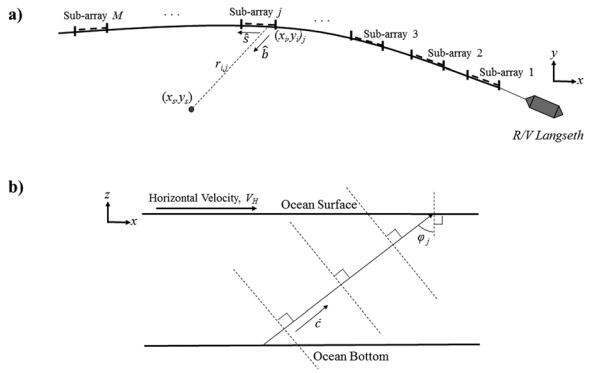

FIG. 3. (a) Cartoon showing the seismic streamer towed behind the *R/V Langseth* with M sub-arrays. The term $r_{i,j}$ is the distance between (x_s, y_s), a selected point in the search grid, and $(x_i, y_i)_j$, the ith element of the jth sub-array, $\vec{b}$ is the unit vector between (x_s, y_s) and $(x_i, y_i)_j$ toward the trial location on the sea surface and $\vec{s}$ is the unit vector along the streamer toward the vessel. (b) Cartoon illustrating a ray path at elevation angle φ_j, and wave fronts (dashed lines). The ray travels with average speed of sound, $\bar{c}$, but the wave front travels with a slower horizontal velocity V_H along the sea surface.

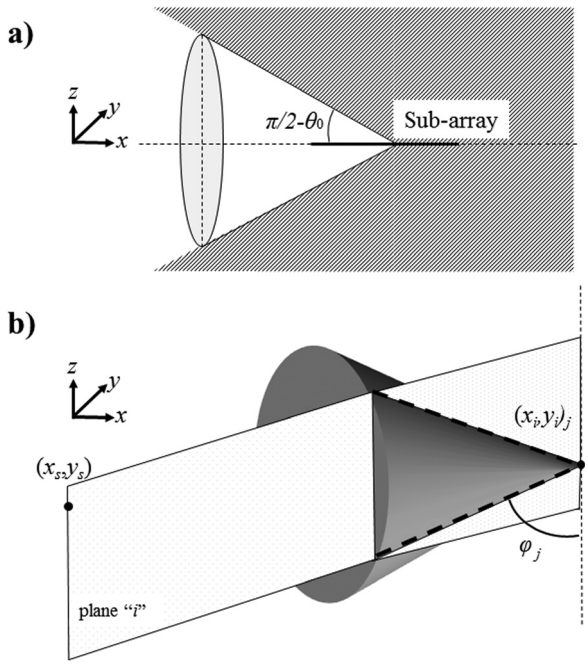

FIG. 4. (a) The beamformer cone for a given ray arrival angle relative to the sub-array, θ_0, (b) the actual arrival path for the trial source location, (x_s, y_s), shown by dashed lines (the intersection between the beamformer cone and the vertical plane "i").

where V_H is the velocity of rays traveling on paths along the sea surface which is termed the horizontal velocity and is equivalent to an average group velocity of modes, and $\varphi_j(x_s, y_s)$ is the elevation angle, the angle between the arrival path and the z axis [see Fig. 3(b)].

All the parameters in Eq. (1) are known or can be found from the environment or the geometry, except $\varphi_j(x_s, y_s)$ which cannot be measured directly. However, the angle of the arrival path relative to the streamer, θ_0, can be calculated from a simple beamforming technique such as the Bartlett beamformer or an adaptive beamforming technique such as the Minimum Variance (MV) beamformer (Jensen *et al.*, 1994). The Bartlett beamformer is the conventional method of beamforming and is calculated according to

$$B_{\mathrm{Bart}}(\theta) = w^{\dagger} K w, \tag{2}$$

where K is the Cross Spectral Density Matrix of the received signal, † denotes the complex transpose operation, and w is the steering column vector whose ith element is $\exp\{i\omega\tau_i(\theta)\}$, with

$$\tau_i(\theta) = (i-1)\left(\frac{d\sin\theta}{\bar{c}}\right), \tag{3}$$

with d the element spacing and θ the beam steering angle with $\theta = 0$ indicating the array's broadside direction.

The MV beamformer is an adaptive spatial filtering technique which suppresses the side lobes and provides an enhanced resolution (see Jensen *et al.*, 1994). The MV beamformer is calculated according to

$$B_{\mathrm{MV}}(\theta) = [w^{\dagger} K^{-1} w]^{-1}. \tag{4}$$

Since the streamer is very long, the plane-wave arrival assumption fails if all the hydrophones are used for beamforming. So, the streamer should be divided into M linear sub-arrays [Fig. 3(a)] with a sufficient number of hydrophones, N_j, to provide a high-resolution beamforming output. The approach to selecting N_j and M is explained in Sec. IV.

Now, the arrival angle calculated from a beamformer technique, θ_0, defines a cone around the sub-array termed the beamformer cone [Fig. 4(a)] which excludes receiver-to-source azimuths outside that cone. The arrival path can be any lateral edge of the beamformer cone. To determine the elevation angle, $\varphi_j(x_s, y_s)$, the actual arrival path must be found. If there is a path between (x_s, y_s) and $(x_i, y_i)_j$, it lies on a plane passing through both points and orthogonal to the ocean bottom [plane "i" shown in Fig. 4(b)]; for simplicity this plane is assumed to be vertical. The arrival path is given by the intersection between the beamformer cone and this plane. The z-component of this intersection yields an estimate of the elevation angle, φ_j,

$$\cos\varphi_j(x_s, y_s) = \sqrt{1 - \frac{(\cos\theta_0)^2}{(\vec{b}\cdot\vec{s})^2}}, \tag{5}$$

where $\vec{b}$ is the unit vector between (x_s, y_s) and $(x_i, y_i)_j$ toward the trial source location on the sea surface and $\vec{s}$ is the unit vector along the streamer toward the vessel [both vectors are shown in Fig. 3(a)]. The elevation angle, $\varphi_j(x_s, y_s)$, and the ray arrival angle, θ_0, are equal only if the arrival path is in the x - z plane. The beamformer cone limits the search area to the region inside the cone which means $\vec{b}\cdot\vec{s} > \cos\theta_0$ for $\theta_0 > 0$ and $\vec{b}\cdot\vec{s} < \cos\theta_0$ for $\theta_0 < 0$.

The ranging approach is to use a grid search method to find the horizontal location that minimizes the normalized rms travel time residual. Grid search methods are commonly used to locate earthquakes and have also been applied to localizing marine mammals (Dunn and Hernandez, 2009;

Wilcock, 2012). To determine the normalized rms travel time residual, the observed arrival time at the first element of the jth sub-array is compared with the calculated travel time between the trial point and $(x_1, y_1)_j$ from Eq. (1). The observed arrival time for the first element of each sub-array is given by $t^o_{1,j} - T_0$. Here $t^o_{1,j}$ is the relative observed time and is found by calculating the maximum cross correlation coefficient between the received signal at $(x_1, y_1)_j$ and a fixed reference element of the streamer, and T_0 is the origin time of the sound relative to the time the sound was recorded at the reference element and can be found from

$$T_0 = \frac{\sum_{j=1}^{M} \frac{\left(t^o_{1,j} - t^c_{1,j}\right)}{\sigma_j^2}}{\sum_{j=1}^{M} \frac{1}{\sigma_j^2}}, \tag{6}$$

where σ_j is the estimate of the time uncertainties or relative uncertainties. The time uncertainties are a combination of the uncertainty in beamforming output (for calculating $t^c_{1,j}$) and cross-correlation output (for calculating $t^o_{1,j}$). The time uncertainty in beamforming output can be estimated from the time difference between the calculated travel time, $t^c_{i,j}$, and the time associated with the arrival angle at 3 dB lower than the highest beamformer value. The time uncertainty in cross-correlation output can be estimated from the average deviation of the relative observed time, $t^o_{1,j}$ from a smooth curve fitted through all the values plotted as a function of distance along the streamer. Here for simplicity, σ_j is chosen as unity and the time uncertainty is estimated after the fact by analyzing the travel time residuals for all locations [see Eq. (9)].

Now, if the selected point is the actual source location, the calculated travel time and observed arrival time at all sub-arrays shown in Fig. 3(a) should be equal. The actual source location is found by finding the point at which the normalized residual time, $R_t(x_s, y_s)$, given by

$$R_t(x_s, y_s) = \sqrt{\frac{1}{M} \sum_{j=1}^{M} \frac{\left(t^o_{1,j} - T_0 - t^c_{1,j}\right)^2}{\sigma_j^2}} \tag{7}$$

is minimum inside the search grid.

The localization uncertainty used in this study is based on a method used for earthquake studies (Wilcock and Toomey, 1991) and previously applied to fin whale locations (Wilcock, 2012). The localization uncertainty is estimated from confidence levels in the spatial residual function $R_t(x_s, y_s)$ derived from the F-statistic

$$R^2_{t,1-\alpha}(x_s, y_s) = \min\left[R^2_t(x_s, y_s)\right] + \frac{p-1}{M} s^2 F(p-1, Q, 1-\alpha), \tag{8}$$

where F denotes the value of F-distribution, p is the number of free parameters in the solution (here $p = 3$: origin time and two horizontal coordinates), Q is given by $Q = \sum_{k=1}^{E} M_k - p$

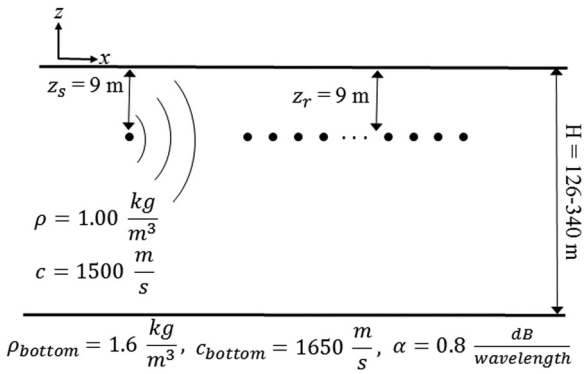

FIG. 5. Array geometry and range-independent Pekeris waveguide model used in simulations that mimic the experiment.

(where E is the number of source localization events and M_k is the number of sub-arrays used in the kth source localization event) and $1-\alpha$ is the confidence level (95% for this study). The term s is a correction factor to the arrival time uncertainties, or an estimate of the average uncertainty itself if σ_j was set to unity in Eq. (6), and is calculated according to

$$s^2 = \frac{\sum_{k=1}^{E} \frac{M_k^2}{M_k - p} \min\left[R^2_{t,k}(x_s, y_s)\right]}{Q}, \tag{9}$$

with $R_{t,k}(x_s, y_s)$ the residual of sub-arrays for the kth source localization event. The location uncertainty is then the maximum distance in the x and y directions between the minimum value of R_t and the contour given by $R_t(x_s, y_s) = R_{t,1-\alpha}(x_s, y_s)$.

IV. RANGING RESULTS FROM SIMULATION

To understand the performance of the sound source localization technique described in Sec. III, a 400 ms chirp is propagated through an environment that mimics the shallow water portion of the experiment (Fig. 5). The normal mode propagation algorithm *KRAKEN* (Porter and Reiss, 1984) is used to propagate a signal through a simple two-layer Perkeris waveguide. Figure 6 shows the group speed of the first six modes; all modes are highly dispersive over this bandwidth which illustrates one of the reasons that the array invariant method (Lee and Makris, 2006) cannot be applied in this study.

Two synthetic sound sources are considered in this section: (1) A 20–80 Hz sound from the airgun location received by a streamer with the configuration shown in Fig. 1(b) propagated through a 126-m-deep water mimicking the geometry presented in Sec. V A, and (2) a 30–50 Hz sound source signal further away and broadside to the streamer propagated through 340 -m-deep water mimicking the geometry during the whale observation presented in Sec. V B. Both sound sources are located at the same depth as the horizontal array (9 m below the surface).

Figure 7 shows the localization result for the airgun simulation using the travel time residual method with Bartlett

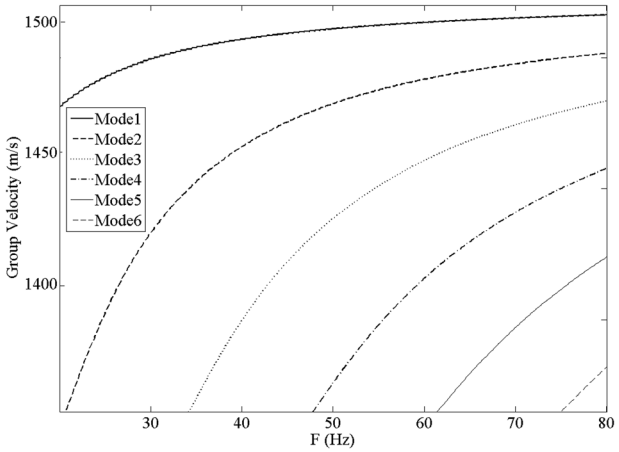

FIG. 6. Group velocities of the first six modes vs frequency calculated by *KRAKEN*, for the environment shown in Fig. 5. It shows that all modes, including mode 1, are dispersive and close to cutoff.

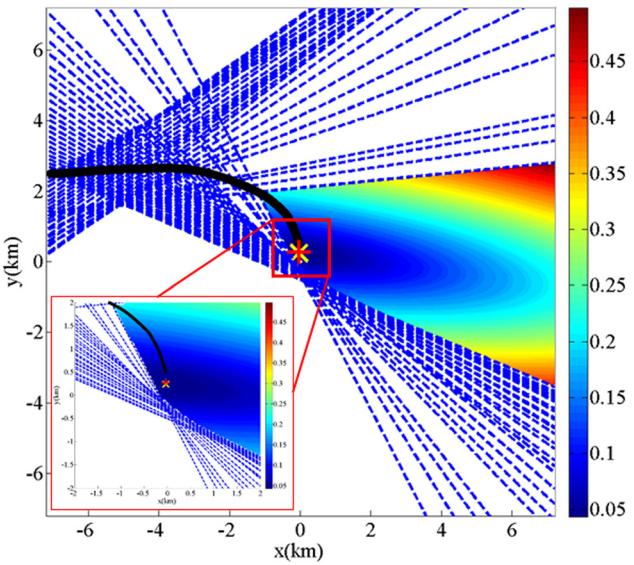

FIG. 7. (Color online) Localization result for a simulated signal in the environment shown in Fig. 5. The source signal has 20–80 Hz bandwidth mimicking the airgun signal. The dashed lines are the lateral edges of the beamformer cone, calculated from the Bartlett beamformer [Eq. (2)], for each selected sub-array. The contour shows the residual travel time (in seconds) using the Bartlett beamformer calculated according to Eq. (7). The solid black line shows the location of the streamer relative to the center of the vessel at the origin. The actual source location (cross mark) and the estimated source location (plus mark) are (−33 m, 238 m) and (−40 m, 272 m), respectively.

beamformer when the SNR is 24.4 dB. As explained in Sec. III, the search area is limited to the intersection of all the sub-arrays' beamformer cones (dashed lines) and the travel time residuals obtained from Eq. (7) are contoured in the allowable area. The estimated source location (plus mark) is (-40 m, 272 m) which differs from the actual airgun location (cross mark) by 34.7 m. This error is likely due to the propagation model mismatch between the localization method (ray approximation) and the simulated received signals (normal mode propagation).

The influence of noise on the airgun localization performance is presented in Table I. Three values of the SNR are considered by adding white noise to the simulated received signals. These results show that (1) the performance of the localization techniques using both beamformers decreases in low SNR, and (2) the MV beamformer yields more accurate locations than Bartlett beamformer.

The number of elements considered in each sub-array are a trade-off between the resolution of the beamformer and the plane-wave arrival. If the number of elements is low, the arrival angle is poorly resolved. On the other hand, a long sub-array will add more errors because: (1) the arrival wave fronts are not planar, and (2) the sub-array will tend to deviate more from a linear array. For Bartlett beamforming, each received signal is shifted by $\tau_i(\theta)$ from Eq. (3) before being summed over number of elements. In a plane wave field, the phase difference between adjacent elements at each frequency should remain constant over the array (Shang and Wang, 1988). To find the optimum number of elements, the variance of the phase difference between two adjoining elements is calculated for different N_j in simulation and shown in Table II. This table shows that a sub-array with 15 elements yields the minimum phase difference variance. Thus, 15 is chosen as the optimum N_j for all the sub-arrays.

Unfortunately, not all the hydrophones can be used for localization because: (1) the assumption of the plane-wave arrival fails for curved parts of the streamer, and (2) the performance of the beamforming techniques decreases when signals arrive from end-fire. For these reasons the red sections shown in Fig. 1(b) are not used in both the simulation and experiment. The number of usable receivers is even lower for the experiment since many elements are noisy.

Figure 8 shows the localization result for the whale call simulation using the travel time residual method with Bartlett beamformer when the SNR is 23.3 dB. The estimated source location (plus mark) is (−4.07 km, −5.95 km) which differs from the actual airgun location (cross mark) by only 86 m. The influence of noise on the localization performance of the simulated whale call is presented in Table III. The localization errors show that the performance of this method decreases for low SNR but the error is still only 110 m for a SNR of 5.2 dB. These results show that the localization technique can be used for narrowband low-frequency

TABLE I. The airgun simulation results using the rms residual travel time technique with the Bartlett and MV beamformers for different values of the SNR. The sound source is a 20–80 Hz signal located at the airgun location. All locations are in (x, y) format.

SNR (dB)	The actual source location (m)	Estimated location–Bartlett beamformer (m)	Localization error–Bartlett beamformer (m)	Estimated location–MV beamformer (m)	Localization error–MV beamformer (m)
24.4	(−33, 238)	(−40, 272)	34.7	(−11, 257)	29.1
10.7	(−33, 238)	(−98, 310)	97.0	(56, 240)	89.0
5.7	(−33, 238)	(−200, 300)	178.1	(−200, 250)	167.4

TABLE II. The variance of the phase difference between adjoining elements in the simulation. The starting element is the 460th element. The SNR is 24.4 dB.

N_j	Phase difference (degree)
5	1.46
10	1.44
15	1.39
20	1.40
25	1.48
30	2.30

sound sources (such as baleen whale vocalization) at significant distances from the streamer when located broadside.

V. RANGING RESULTS FROM 2012 COAST EXPERIMENT

The localization technique has been applied to two types of signal from the COAST experiment. The first, airguns, have a known source location and thus can be used to ground-truth the method. The second, whale calls, are the signal of interest but the locations are harder to ground truth accurately, because the visual observations are only approximate and are made at times that may not coincide with the time of a vocalization or the actual whale that vocalized.

A. Airgun localization

The data analyzed here were collected during the turns between survey lines when the mitigation gun was fired.

1. Shallow water

A total of 11 shots in shallow water are considered. The localization results are listed in Table IV. All shots were recorded during the turn between line 5 and 7 [Fig. 1(a)] on July 16, 2012 between 17:56:36 and 18:01:26 and the water depth varies between 125 and 129 m. Figure 9 shows the localization result for the seventh shot in Table IV using (a) the Bartlett and (b) the MV beamformer. The bandwidth of 20–80 Hz is used for both beamforming results. The estimated source locations (plus marks) are (-36 m, 290 m) for the Bartlett beamformer and (-72 m, 204 m) for the MV beamformer which differ from the actual airgun location (cross marks) by 52.1 and 51.7 m, respectively.

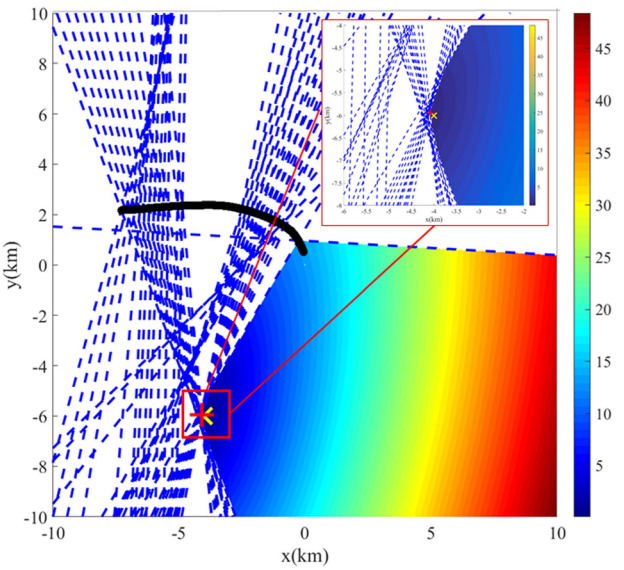

FIG. 8. (Color online) Localization result for the simulated whale call in an environment shown in Fig. 5 plotted with the same conventions as Fig. 7. The source signal has a 30–50 Hz bandwidth mimicking a whale call. The actual source location (cross mark) and the estimated source location (plus mark) are (−4.00 km, −6.00 km) and (−4.07 km, −5.95 km), respectively.

The rms location error, e_{rms} is given by

$$e_{\text{rms}} = \left[\frac{1}{E}\sum_{i=1}^{E} \|\vec{x}_{\text{estimated}} - \vec{x}_{\text{actual}}\|_i^2\right]^{1/2}, \quad (10)$$

where $\vec{x}_{\text{estimated}}$ is an estimated location, $\vec{x}_{\text{actual}}$ is the actual location, i is the location index, and E is the total number of locations. For the shots in Table IV the rms location errors are 160 m, and 89 m for the Bartlett beamforming and MV beamforming techniques, respectively, when 20–80 Hz bandwidth is selected for the calculation. These values are 3%, and 1.5% of the average range between the airgun and all receivers, 5.9 km. Here, the estimated locations using the MV beamformer are more accurate than the estimated locations using the Bartlett beamformer. The reason is that the MV beamformer is more efficient in suppressing side lobes when frequencies are higher than the design frequency.

When a higher bandwidth of 80–140 Hz is used for the calculation, the rms location errors are 185 and 140 m for the Bartlett and MV beamforming techniques, respectively. Since these frequencies are much higher than the design frequency of the streamer (∼60 Hz), there are more side lobes in beamforming outputs and the arrival angle calculation is less accurate. Since the airgun signature is dominated by energy between 20 and 80 Hz and the beamforming outputs are less ambiguous at this frequency range, only 20–80 Hz bandwidth is considered for deep water calculation in Sec. V A 2.

2. Deep water

A total of eight shots in deep water are analyzed and the results are presented in Table V. All these shots were recorded on July 20, 2012 between 16:17:41 and 16:20:41. Figure 10 shows the localization details for the fifth shot in Table V. The rms location errors [Eq. (10)] using all shots in Table V are 373 and 304 m for Bartlett beamforming and MV beamforming techniques, respectively. The localization results show that this technique is less accurate in deep water. This is likely because the ocean thermocline refracts rays so that the horizontal velocity inferred from the arrival angle at the streamer at shallow depths is not representative of the average horizontal velocity over the full water depth.

B. Whale localization

Although many humpback whales were observed in the survey area, just a few whale calls were found in the streamer data. There are two possible reasons for this: (1) the whales were not vocalizing at the time, and (2) any

TABLE III. The whale call simulation results using the rms residual travel time technique with the Bartlett and MV beamformers for different values of the SNR. The sound source is a 3050 Hz signal broadside to the streamer mimicking a whale vocalization. All locations are in (x, y) format, relative to the center of the vessel.

SNR (dB)	The actual source location (km)	Estimated location–Bartlett beamformer (km)	Localization error–Bartlett beamformer (km)	Estimated location–MV beamformer (km)	Localization error–MV beamformer (km)
23.3	(−4.00, −6.00)	(−4.07, −5.95)	0.08	(−4.05, −6.00)	0.05
11.5	(−4.00, −6.00)	(−4.10, −6.00)	0.1	(−4.07, −5.95)	0.08
5.2	(−4.00, −6.00)	(−4.10, −5.95)	0.11	(−4.10, −5.95)	0.11

vocalizations made were at frequencies higher than 220 Hz and thus are not visible in the hydrophone spectrograms.

A total of 8 low frequency vocalizations (20–60 Hz) were detected on the streamer data recorded on July 16, 2012 between 19:38:55 and 21:29:39 in ∼340-m-deep water (Table VI). The first recording occurred when no airgun was fired, while the mitigation gun was on during the other recordings. Figure 11 shows the localization results using the MV beamformer for the calls shown in Figs. 2(b) and 2(c). The estimated locations (plus marks) are (7.25 km, 17.50 km) and (7.75 km, 18.00 km), respectively, from the center of the vessel.

These recordings come soon after a period when 12 humpback whales (11 adults and 1 juvenile) were observed by the PSOs for 40 min between 18:29:00 and 19:12:00 with locations reported twice and overlap two more sightings of individual humpback whales (20:30:00 and 20:53:00). Since these signals are within the same frequency band as the airgun signal, it is important to consider whether they are environmental reverberations. If these signals were environmental reverberations, they should be consistently present at the same time relative to the airgun pulses in sequences of closely spaced shots, but this is not seen. As an example, Fig. 12 shows that the 30–50 Hz signal recorded at 21:25:08 is not recorded on shots 30 s earlier and 29 s later. In addition, the recorded time of the signals is uncorrelated with the airgun pulses. For instance, the 30–50 Hz signal is recorded ∼6 s after the airgun signal in Fig. 2(b), ∼11 s after the airgun signal in Fig. 2(c), and ∼5 s before the airgun signal in Fig. 12(b). Moreover, on one occasion it was recorded even when the mitigation gun was off (the first signal in Table VI).

These 30–50 Hz signals are at frequencies similar to known 16 Hz calls of the northeast Pacific blue whale (Stafford *et al.*, 1998) but their duration is too short. They could be from the observed humpback whales; humpbacks normally vocalize at higher frequencies (Thompson *et al.*, 1986) but a similar recording has been reported by Paul J. Perkins at Macaulay Library (http://macaulaylibrary.org/audio/117268–March 19, 1978 at 12:24 in the recorded file). However, there is not enough information available to prove this hypothesis.

Figure 13 shows the spatial distribution in Universal Transverse Mercator (UTM) coordinates of all the recorded

TABLE IV. The shallow water airgun localization results using the rms residual travel time technique with Bartlett and MV beamforming technique. All locations are in (x, y) format, relative to the center of the vessel. All shots were recorded on July 16, 2012.

Shot number	Recorded time	Water depth (m)	The actual location of the airgun (m)	Bandwidth (Hz)	Estimated location using rms residual travel time technique (Bartlett beamformer) (m)	Estimated location using rms residual travel time technique (MV beamformer) (m)
1	17:56:36	125	(−35, 236)	20–80	(−200 ± 14, 382 ± 36)	(−96 ± 106, 190 ± 46)
				80–140	(−86 ± 21, 310 ± 41)	(−30 ± 18, 228 ± 43)
2	17:57:24	127	(−33, 238)	20–80	(−194 ± 89, 316 ± 44)	(−70 ± 96, 214 ± 48)
				80–140	(−22 ± 10, 352 ± 31)	(78 ± 12, 154 ± 24)
3	17:58:11	126	(−31, 238)	20–80	(−154 ± 20, 348 ± 40)	(−60 ± 98, 224 ± 48)
				80–140	(19 ± 24, 296 ± 38)	(74 ± 21, 170 ± 41)
4	17:58:35	126	(−34, 239)	20–80	(–138 ±54, 274 ± 26)	(−116 ± 48, 214 ± 22)
				80–140	(130 ± 57, −12 ± 53)	(88 ± 65, 64 ± 58)
5	17:58:59	127	(−34, 239)	20–80	(−94 ± 50, 186 ± 46)	(−104 ± 20, 138 ± 32)
				80–140	(36 ± 31, 130 ± 52)	(−18 ± 24, 116 ± 41)
6	17:59:23	126	(−33, 239)	20–80	(32 ± 54, 212 ± 28)	(−100 ± 46, 202 ± 22)
				80–140	(144 ± 54, 8±64)	(104 ± 58, 84 ± 63)
7	17:59:47	126	(−33, 238)	20–80	(−36 ± 94, 290 ± 54)	(−72 ± 86, 204 ± 50)
				80–140	(−92 ± 41, 370 ± 50)	(−8 ± 54, 370 ± 50)
8	18:00:12	128	(−32, 240)	20–80	(−120 ± 20, 240 ± 32)	(−152 ± 68, 194 ± 38)
				80–140	(160 ± 61, 32 ± 75)	(92 ± 58, 72 ± 77)
9	18:00:36	128	(−32, 240)	20–80	(−184 ± 12, 390 ± 32)	(−132 ± 34, 204 ± 30)
				80–140	(−46 ± 26, 346 ± 45)	(26 ± 42, 192 ± 34)
10	18:01:01	129	(−31, 241)	20–80	(−96 ± 46, 232 ± 50)	(−16 ± 72, 102 ± 40)
				80–140	(120 ± 52, 104 ± 74)	(40 ± 49, 266 ± 34)
11	18:01:26	127	(−30, 243)	20–80	(−208 ± 10, 486 ± 16)	(−26 ± 38, 252 ± 22)
				80–140	(−56 ± 22, 308 ± 52)	(−6 ± 31, 190 ± 57)

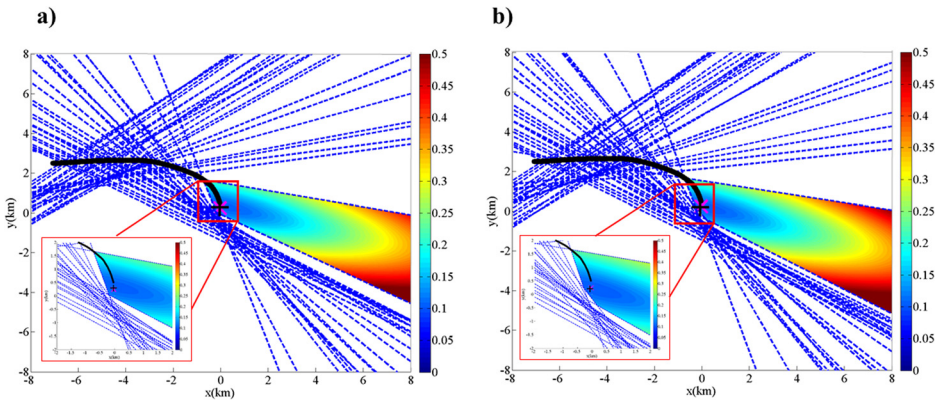

FIG. 9. (Color online) Shallow water localization results for the seventh shot in Table IV plotted using the same conventions as Fig. 7 obtained from (a) the Bartlett beamformer [Eq. (2)] and (b) the MV beamformer [Eq. (4)]. The estimated source locations are (−36 m, 290 m) and (−72 m, 204 m) for the Bartlett and MV beamformers, respectively.

TABLE V. The deep water airgun localization results using the rms residual travel time technique with Bartlett and MV beamforming technique. All locations are in (x, y) format, relative to the center of the vessel. All shots were recorded on July 20, 2012.

Shot number	Recorded time	Water depth (m)	The actual location of the airgun (m)	Estimated location using rms residual travel time technique (Bartlett beamformer) (m)	Estimated location using rms residual travel time technique (MV beamformer) *(m)*
1	16:17:41	2602	(51, −212)	(490 ± 25, −440 ± 10)	(280 ± 20, −330 ± 15)
2	16:18:05	2600	(51, −213)	(445 ± 25, −400 ± 15)	(360 ± 20, −470 ± 15)
3	16:18:28	2599	(51, −213)	(300 ± 20, −285 ± 10)	(225 ± 20, −290 ± 10)
4	16:18:54	2600	(51, −213)	(95 ± 25, −300 ± 15)	(150 ± 20, −285 ± 10)
5	16:19:21	2600	(50, −214)	(290 ± 25, −360 ± 15)	(240 ± 20, −360 ± 10)
6	16:19:49	2599	(49, −214)	(305 ± 25, −355 ± 15)	(340 ± 20, −410 ± 10)
7	16:20:16	2601	(47, −214)	(445 ± 25, −480 ± 15)	(355 ± 25, −435 ± 15)
8	16:20:41	2600	(46, −214)	(430 ± 25, −455 ± 10)	(370 ± 20, −385 ± 10)

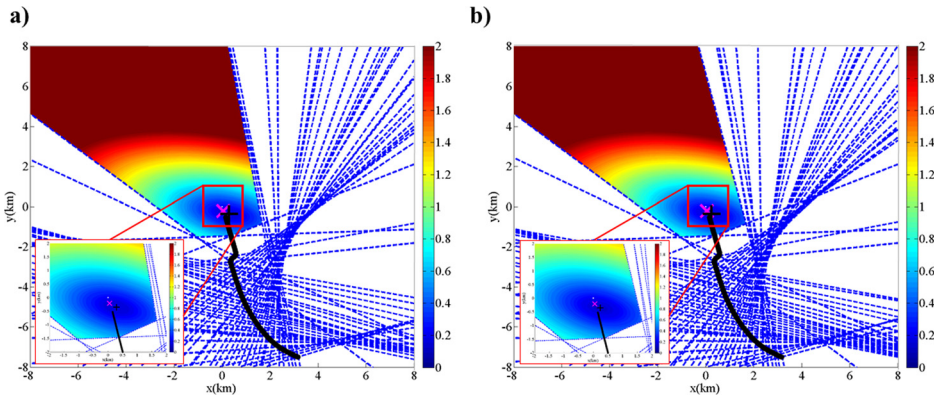

FIG. 10. (Color online) Deep water localization results for the fifth shot in Table V plotted with the same conventions as Fig. 9. The estimated source locations are (290 m, −360 m) and (240 m, −360 m) for the Bartlett and MV beamformers, respectively.

TABLE VI. The whale call localization results. All locations are in (x, y) format, relative to the center of the vessel at the time of the call. All calls are recorded on July 16, 2012.

Signal #	Recorded time	Water depth (m)	Airgun status	Estimated location using rms residual travel time technique (Bartlett beamformer) (km)	Estimated location using rms residual travel time technique (MV beamformer) (km)
1	19:38:55	124	Off	(−0.20 ± 0.45, 5.50 ± 0.20)	(−0.25 ± 0.50, 5.50 ± 0.15)
2	21:06:11	333	Mitigation gun	(7.10 ± 0.10, 16.50 ± 0.40)	(7.25 ± 0.10, 17.50 ± 0.10)
3	21:09:03	274	Mitigation gun	(8.00 ± 0.10, 16.50 ± 0.10)	(7.75 ± 0.10, 18.00 ± 0.10)
4	21:13:20	286	Mitigation gun	(9.75 ± 0.10, 19.75 ± 0.10)	(9.00 ± 0.10, 19.25 ± 0.25)
5	21:17:43	325	Mitigation gun	(9.75 ± 0.10, 21.00 ± 0.10)	(10.00 ± 0.10, 21.50 ± 0.10)
6	21:24:07	340	Mitigation gun	(10.25 ± 0.25, 13.75 ± 0.75)	(10.50±0.10, 14.50±0.10)
7	21:25:08	337	Mitigation gun	(11.00 ± 0.25, 20.25 ± 1.25)	(11.50 ± 0.25, 23.25 ± 0.75)
8	21:29:39	342	Mitigation gun	(11.50 ± 0.25, 18.50 ± 1.00)	(11.75 ± 0.10, 19.25 ± 0.10)

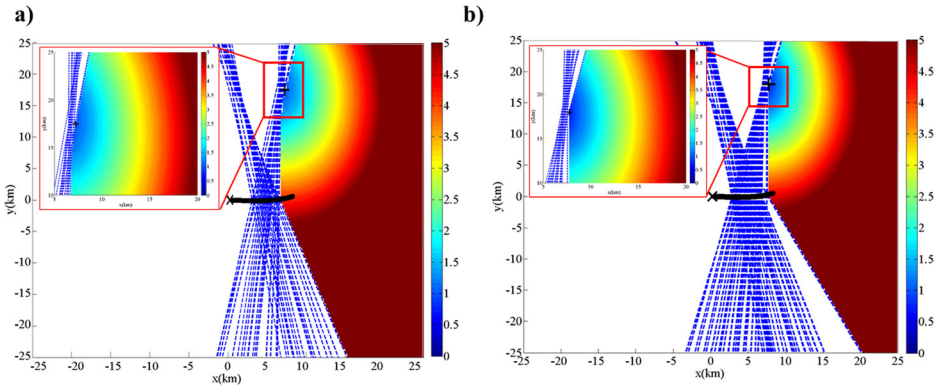

FIG. 11. (Color online) (a) Whale localization result for the call shown in Fig. 2(b) plotted with the same conventions as Fig. 7 using the MV beamforming technique. The estimated location is (7.25 km, 17.50 km) from the center of the vessel, and (b) whale localization result for the call in shown in Fig. 2(c) plotted with the same conventions as Fig. 7 using the MV beamforming technique. The estimated location is (7.75 km, 18.00 km) from the center of the vessel.

signals with MV beamforming and also the locations of four observations as reported by the PSOs. The first acoustic detection happened at 19:38:55 and was localized about 5.5 km from the vessel and is reasonably consistent with the second visual location reported for humpback whales at 19:12:00. Unfortunately, no data were recorded between 19:38:55 and 21:02:05 when two more visual observations were made for humpbacks near the vessel. When recording resumed, 7 signals were recorded in about 23 min and are located 19–26 km from the vessel, well outside the range of visual observations.

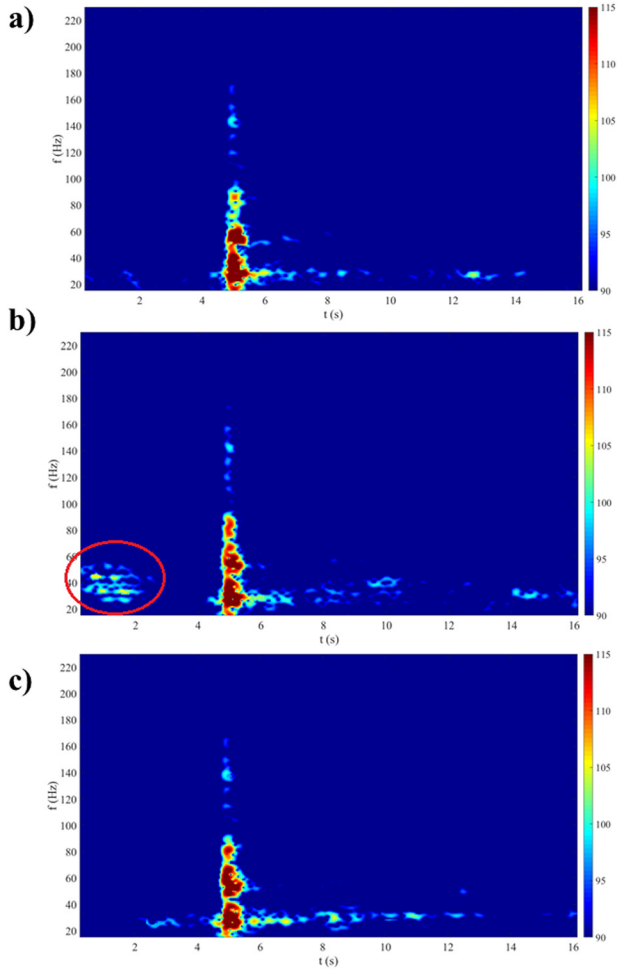

FIG. 12. (Color online) (a) Spectrogram of the mitigation gun recorded 30 s before the seventh shot in Table VI, (b) spectrogram of the seventh whale signal in Table VI followed by the airgun signal, and (c) spectrogram of the mitigation gun recorded 29 s after the seventh shot in Table VI. All spectrograms are recorded by the same hydrophone located 7.38 km from the center of the vessel.

VI. CONCLUSIONS

The performance of a low frequency sound source localization technique using the data recorded by a seismic streamer has been investigated. This method uses the Bartlett or MV beamforming techniques to minimize the error between the calculated travel time and observed arrival time on a search grid. The localization results indicate that MV beamforming increases the accuracy of the estimated location compared to Bartlett beamforming and that the localizations are more accurate in shallow water. Since the method uses the ray approximation for sound propagation in this environment, the localization error is likely to increase as the range of the source normalized to the water depth increases (Jensen *et al.*, 1994).

It has been shown that this method could be used to locate vocalizations from baleen whales recorded by the seismic streamer. This may be important for passive studies of baleen whales' behavior during seismic surveys. Whale calls can be recorded within a large area around the airgun array and they can be localized at night or in poor weather conditions that are not conducive to visual surveys. Studying

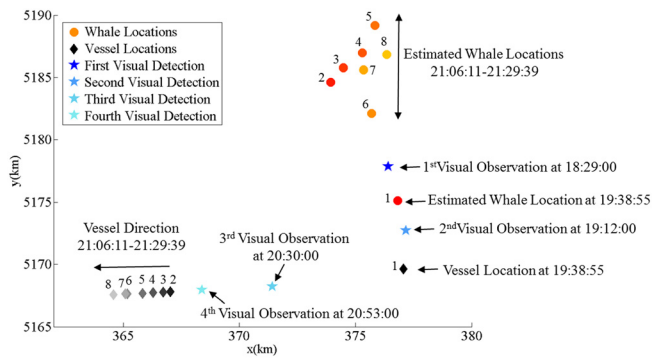

FIG. 13. (Color online) Spatial distribution in UTM coordinates of recorded calls presented in Table VI. The estimated locations using the travel time residual technique with MV beamforming are shown by circles, color coded in time (the numbers are the call numbers in Table VI). Four visual detections reported by the marine mammal during the same interval is shown by stars. The locations of *R/V Langseth* when calls were recorded by the streamer are shown by diamonds. For calls 2–8 the vessel was located further west.

the impact of seismic surveys on baleen whales may be possible by locating them before, during, and after the seismic survey. Also, the use of streamer data could help marine mammal observers verify the accuracy of visual whale detections and range estimates during seismic experiments.

ACKNOWLEDGMENTS

We thank Kate Stafford for her help in whale call identification. We also thank two anonymous reviewers, and associate editor Aaron Thode for thorough reviews which substantially improved the manuscript. Furthermore, we thank the captain, crew, and technical and science party for *R/V Marcus Langseth* cruise MGL1212. This work was supported by the National Science Foundation under Grant No. OCE12-14328.

Abadi, S. H., Thode, A. M., Blackwell, S. B., and Dowling, D. R. (**2014**). "Ranging bowhead whale calls in a shallow-water dispersive waveguide," J. Acoust. Soc. Am. **136**, 130–144.

Barlow, J., and Taylor, B. L. (**2005**). "Estimates of sperm whale abundance in the Northeastern temperate Pacific from a combined acoustic and visual survey," Mar. Mammal Sci. **21**(3), 429–445.

Bassett, C., Polagye, B., Holt, M., and Thomson, J. (**2012**). "A vessel noise budget for Admiralty Inlet, Puget Sound, Washington (USA)," J. Acoust. Soc. Am. **132**, 3706–3719.

Bucker, H. P. (**1976**). "Use of calculated sound field for matched field detection to locate sound source in shallow water," J. Acoust. Soc. Am. **59**, 368–373.

Clark, C. W., and Ellison, W. T. (**2000**). "Calibration and comparison of the acoustic location methods used during the spring migration of the bowhead whale, Balaena mysticetus, off Pt. Barrow, Alaska, 1984-1993," J. Acoust. Soc. Am. **107**(6), 3509–3517.

Cockrell, K. L., and Schmidt, H. (**2010**). "Robust passive range estimation using the waveguide invariant," J. Acoust. Soc. Am. **127**, 2780–2789.

Crone, T. J., Tolstoy, M., and Carton, H. (**2014**). "Estimating sound power levels and mitigation radii for the R/V Marcus G. Langseth using an 8-km long MCS streamer," Geochem. Geophys. Geosyst. **15**, 3793–3807.

Diebold, J. B., Tolstoy, M., Doermann, L., Nooner, S. L., Webb, S. C., and Crone, T. J. (**2010**). "R/V *Marcus G. Langseth* seismic source: Modeling and calibration," Geochem. Geophys. Geosyst. **11**, Q12012.

Dunn, R. A., and Hernandez, O. (**2009**). "Tracking blue whales in the eastern tropical Pacific with an ocean-bottom seismometer and hydrophone array," J. Acoust. Soc. Am. **126**, 1084–1094.

Gong, Z., Jain, A. D., Tran, D., Yi, D. H., Wu, F., Zorn, A., Ratilal, P., and Makris, N. C. (**2014**). "Ecosystem scale acoustic sensing reveals humpback whale behavior synchronous with herring spawning processes and re-evaluation finds no effect of sonar on humpback song occurrence in the Gulf of Maine in Fall 2006," PLoS ONE **9**(10), e104733.

Gong, Z., Tran, D. D., and Ratilal, P. (**2013**). "Comparing passive source localization and tracking approaches with a towed horizontal receiver array in an ocean waveguide," J. Acoust. Soc. Am. **134**, 3705–3720.

Gordon, J., Gillespie, D., Potter, J., Frantzis, A., Simmonds, A. P., Swift, R., and Thompson, D. (**2004**). "A review of the effects of seismic surveys on marine mammals," Mar. Technol. Soc. J. **37**, 16–34.

Greene, C. R., McLennan, M. W., Norman, R. G., Mcdonald, T. L., Jakubczak, R. S., and Richardson, W. J. (**2004**). "Directional frequency and recording (DIFAR) sensors in seafloor recorders to locate calling bow-head whales during their fall migration," J. Acoust. Soc. Am. **116**, 799–813.

Holbrook, S., Kent, G., Keranen, K., Johnson, P., Trehu, A., Tobin, H., Caplan-Auerbach, J., and Beeson, J. (**2012**). "COAST: Cascadia Open-Access Seismic Transects," GeoPRISMS Newsletter Vol. 29.

Jensen, F., Kuperman, W., Porter, M., and Schmidt, H. (**1994**). *Computational Ocean Acoustics* (American Institute of Physics, New York), Chaps. 3 and 10.

Kinsler, L. E., Frey, A. R., Coppens, A. B., and Sanders, J. V. (**2000**). *Fundamentals of Acoustics*, 4th ed. (Wiley, New York), Chap. 5.

Lee, S., and Makris, N. C. (**2006**). "The array invariant," J. Acoust. Soc. Am. **119**, 336–351.

Li, S., Akamatsu, T., Wang, D., and Wang, K. (**2009**). "Localization and tracking of phonating finless porpoises using towed stereo acoustic data-loggers," J. Acoust. Soc. Am. **126**(1), 468–475.

Lin, Y. T., Newhall, A. E., and Lynch, J. F. (**2012**). "Low-frequency broadband sound source localization using an adaptive normal mode back-propagation approach in a shallow-water ocean," J. Acoust. Soc. Am. **131**, 1798–1813.

McDonald, M. A., and Fox, C. G. (**1999**). "Passive acoustic methods applied to fin whale population density estimation," J. Acoust. Soc. Am. **105**, 2643–2651.

McDonald, M. A., Hildebrand, J. A., and Webb, S. C. (**1995**). "Blue and fin whales observed on a seafloor array in the Northeast Pacific," J. Acoust. Soc. Am. **98**, 712–721.

McKenna, M., Ross, D., Wiggins, S., and Hildebrand, J. (**2012**). "Underwater radiated noise from modern commercial ships," J. Acoust. Soc. Am. **131**, 92–103.

Nosal, E. M. (**2013**). "Methods for tracking multiple marine mammals with wide-baseline passive acoustic arrays," J. Acoust. Soc. Am. **134**, 2383–2392.

Nosal, E. M., and Frazer, L. N. (**2006**). "Track of a sperm whale from delays between direct and surface-reflected clicks," Appl. Acoust. **67**, 1187–1201.

Pedersen, M. A., and Gordon, D. F. (**1965**). "Normal-mode theory applied to short-range propagation in an underwater acoustic surface duct," J. Acoust. Soc. Am. **37**(1), 105–118.

Perkins, P. J. (**1978**). http://macaulaylibrary.org/audio/117268 - March 19, 1978 at 12:24 in the recorded file (Last viewed 2/24/2015).

Porter, M. B., and Reiss, E. L. (**1984**). "A numerical method for ocean acoustic normal modes," J. Acoust. Soc. Am. **76**, 244–252.

Richardson, W. J., Greene, C. R., Jr., Malme, C. L., and Thomson, D. H. (**1995**). *Marine Mammals and Noise* (Academic Press, New York), Chap. 6.

Shang, E., and Wang, Y. (**1988**). "Acoustic source bearing modeling in shallow water waveguides," Math. Comp. Model. **11**, 1052–1055.

Song, H. C., and Cho, C. (**2015**). "The relation between the waveguide invariant and array invariant," J. Acoust. Soc. Am. **138**, 899–903.

Speisberger, J. L., and Fristrup, K. M. (**1990**). "Passive location of calling animals and sensing of their acoustic environment using acoustic tomography," Am. Nat. **135**, 107–153.

Stafford, K. M., Fox, C. G., and Clark, D. S. (**1998**). "Long-range acoustic detection and localization of blue whale calls in the northeast Pacific Ocean," J. Acoust. Soc. Am. **104**(6), 3616–3625.

Thode, A. (**2005**). "Three-dimensional passive acoustic tracking of sperm whales (Physeter macrocephalus) in ray-refracting environments," J. Acoust. Soc. Am. **118**(6), 3575–3584.

Thode, A. M. (**2004**). "Tracking sperm whale (Physeter macrocephalus) dive profiles using a towed passive acoustic array," J. Acoust. Soc. Am. **116**(1), 245–253.

Thode, A. M., D'Spain, G. L., and Kuperman, W. A. (**2000**). "Matched-field processing and geoacoustic inversion of blue whale vocalizations," J. Acoust. Soc. Am. **107**, 1286–1300.

Thode, A. M., Gerstoft, P., Burgess, W. C., Sabra, K. G., Guerra, M., Stokes, D. M., Noad, M., and Cato, D. H. (**2006**). "A portable matched-field processing system using passive acoustic time synchronization," IEEE J. Ocean Eng. **31**, 696–710.

Thode, A. M., Kim, K. H., Blackwell, S. B., Greene, C. R., McDonald, T. L., and Macrander, M. A. (**2012**). "Automated detection and localization of bowhead whale sounds in the presence of seismic airgun surveys," J. Acoust. Soc. Am. **131**, 3726–3747.

Thompson, P. O., Cummings, W. C., and Ha, S. J. (**1986**). "Sounds, source levels, and associated behavior of humpback whales, Southeast Alaska," J. Acoust. Soc. Am. **80**, 735–740.

Tiemann, C., Thode, A., Straley, J., O'Connell, V., and Folkert, K. (**2006**). "Three-dimensional localization of sperm whales using a single hydrophone," J. Acoust. Soc. Am. **120**, 2355–2365.

Tolstoy, M., Diebold, J. B., Webb, S. C., Bohnenstiehl, D. R., Chapp, E., Holmes, R. C., and Rawson, M. (**2004**). "Broadband calibration of the R/V Ewing seismic sources," Geophys. Res. Lett. **31**, L14310, doi:10.1029/2004GL020234.

Tolstoy, M., Diebold, J. B., Doermann, L., Nooner, S., Webb, S. C., Bohnenstiehl, D. R., Crone, T. J., and Holmes, R. C. (**2009**). "Broadband calibration of the R/V Marcus G. Langseth four-string seismic sources," Geochem., Geophys. Geosyst. **10**, Q08011, doi:10.1029/2009GC002451.

Tran., D. D., Huang, W., Bohn, A. C., Wang, D., Gong, Z., Makris, N. C., and Ratila, P. (**2014**). "Using a coherent hydrophone array for observing

sperm whale range, classification, and shallow-water dive profiles," J. Acoust. Soc. Am. **135**(6), 3352–3363.
von Benda-Beckmann, A. M., Beerens, S. P., and van Ijsselmuide, S. P. (**2013**). "Effect of towed array stability on instantaneous localization of marine mammals," J. Acoust. Soc. Am. **134**(3), 2409–2417.
Wiggins, S. M., McDonald, M. A., Munger, L. A., Hildebrand, J. A., and Moore, S. E. (**2004**). "Waveguide propagation allows range estimates for North Pacific right whales in the Bering Sea," Can. Acoust. **32**, 146–154.
Wilcock, W. S. (**2012**). "Tracking fin whales in the northeast Pacific Ocean with a seafloor seismic network," J. Acoust. Soc. Am. **132**(4), 2408–2419.
Wilcock, W. S. D., and Toomey, D. R. (**1991**). "Estimating hypocentral uncertainties from marine microearthquake surveys: A comparison of generalized inverse and grid search methods," Mar. Geophys. Res. **13**, 161–171.
Yardim, C., Michalopoulou, Z., and Gerstoft, P. (**2011**). "An overview of sequential Bayesian filtering in ocean acoustics," IEEE J. Ocean Eng. **36**, 71–89.